AJNR

Cholesterol granuloma of the petrous apex: MR and CT evaluation.

J J Greenberg, R F Oot, G L Wismer, K R Davis, M L Goodman, A E Weber and W W Montgomery

Cholesterol Granuloma of the Petrous Apex: MR and CT Evaluation

Jeffrey J. Greenberg[1,2]
Robert F. Oot[1,3]
Gary L. Wismer[1,4]
Kenneth R. Davis[1]
Max L. Goodman[5]
Alfred E. Weber[6]
William W. Montgomery[7]

We reviewed the clinical, CT, and MR findings in seven consecutive patients who had a total of nine cholesterol granulomas. Preoperative MR scans were available for five of the seven patients; two patients were studied with MR after treatment only (one had a recurrent lesion and the other was asymptomatic at the time of study). Preoperative CT scans were available for all patients, except one patient who was examined after developing a symptomatic recurrence. All lesions were detected by both imaging methods. Seven preoperative lesions (five patients) and one symptomatic recurrence (one patient) demonstrated increased signal intensity of both T1- and T2-weighted MR images. Three surgically drained lesions (three patients) showed a marked reduction in signal intensity on T1-weighted images. Pre- and postoperative lesions had different patterns of signal intensity on the chemical-shift images, which were obtained in two instances. The MR appearance of cholesterol granuloma differs from that of most other lesions that occur in the petrous apex. CT did not differentiate between pre- and postoperative lesions in all cases, while MR demonstrated a dramatic change on T1-weighted images and chemical-shift studies.

Our findings indicate that MR is more specific than CT in suggesting the correct diagnosis of cholesterol granuloma and that MR appears to be the technique of choice in the follow-up of previously treated patients.

Cholesterol granulomas of the petrous apex are slowly growing, extradural lesions that represent an inflammatory granulation tissue response to the presence of cholesterol crystals [1–4]. These expansile lesions probably arise as a result of recurrent hemorrhage into pneumatized and obstructed air cells in the petrous apex [2–4]. Clinically, the patients usually present with cerebellopontine angle syndrome [5–10], suggesting a sizable lesion. In contrast to other lesions that occur in this location and require extensive surgery, effective treatment of cholesterol granulomas generally can be performed by a relatively simple drainage and permanent fistulization procedure [5–10]. Thus, accurate preoperative diagnosis of cholesterol granuloma is important in evaluating patients for surgery.

Although CT has been the primary mode of radiologic diagnosis of this lesion, the appearance, while characteristic, is not very specific. We investigated the capability of MR imaging in providing better diagnostic specificity in a series of seven consecutive patients who had a total of nine granulomas.

Materials and Methods

Seven patients, four men and three women, 29–53 years old, with symptomatic expansile lesions of the petrous apex were studied by MR and CT. Clinical data are summarized in Table 1. Surgical confirmation of the diagnosis of cholesterol granuloma was obtained in five patients. All patients initially had neurologic symptoms; the duration of signs and symptoms was 3–96 months. The most common symptom was eighth nerve dysfunction, which occurred in four cases. Three of seven patients experienced fifth nerve abnormalities, including facial pain and paresthesias; and three had sixth nerve palsy, manifesting as transient diplopia.

TABLE 1: Clinical Findings in Seven Patients with Cholesterol Granulomas Who Were Studied with MR and CT

Case No.	Age at Clinical Presentation	Gender	Date of Diagnosis	Signs and Symptoms at Clinical Presentation	Location of Lesion	MR Images	CT Scans	Confirmed by Surgery
1	42	M	6/74	Symptomatic recurrence 12 years after initial treatment. Original tumor was preceded by 8 years of facial paresthesias (R), 2 years of decreased hearing (R), 1 month of sixth nerve palsy (R), and decreased taste (R side of tongue)	R	Postop	Postop	Yes
2	49	F	5/78	8 years of positional vertigo, 3 months of otalgia (R), and decreased gag reflex (R)	R	Postop	Pre- and postop	Yes
3	53	F	3/84	2 years of facial paresthesias (L) and 1 year of sixth nerve palsy (L)	L	Preop	Preop	No
4	45	M	10/85	3 months of facial paresthesias (L) and 1 month of decreased hearing (L)	L	Pre- and postop	Pre- and postop	Yes
5	40	M	11/85	4 months of decreased hearing and otalgia (L) and 1 month of hemifacial spasm (L)	Bilateral (L > R)	Preop	Preop	No
6	30	M	9/86	3 years of facial paresis (R), 3 months of decreased hearing (R) and sixth nerve palsy (R)	Bilateral (R > L)	Pre- and postop	Preop	Yes
7	29	F	12/86	1 year of dysequilibrium	R	Preop	Preop	Yes

Note.—R = right, L = left; Postop = postoperative; Preop = preoperative.

Two patients experienced seventh nerve abnormalities—one with hemifacial spasm and the second with a peripheral facial palsy. Other, less specific symptoms included headache, otalgia, dysequilibrium, diminished gag reflex, and absent taste on one side of the tongue.

Preoperative MR images were obtained in five clinically symptomatic patients (cases 3–7, Table 1). Two of these patients (cases 4 and 6) also had postoperative MR examinations after successful drainage of the lesions. One patient (case 4) was examined 2 months after surgery, while the other (case 6) was examined 2½ weeks after surgery. Two patients (cases 1 and 2) were studied only after treatment. One of these (case 1) was examined by MR after becoming symptomatic from a recurrence of a granuloma that was initially treated 12 years earlier. The other (case 2) had undergone treatment 8 years before and was asymptomatic when examined by MR.

Preoperative CT images were obtained in six clinically symptomatic patients (cases 2–7). Two of these patients (cases 2 and 4) also had several postoperative CT examinations after successful surgical drainage of the lesions. The seventh patient (case 1) was studied by CT only after developing a symptomatic recurrence that originally was treated 12 years before.

MR examinations were performed on a whole-body system with a superconducting magnet operating at a field strength of 0.6 T. All images were acquired with a 26-cm-diameter head coil. Images were obtained with 128 phase-encoding (y gradient) steps, interpolated to 256 for image display. In the x dimension, 256 frequency-encoding steps were used, resulting in a display matrix of 256 × 256. Nominal in-plane spatial resolution was 2.0 × 1.0 mm. In all patients, axial T1- and T2-weighted images were obtained. The axial images were supplemented in all cases by either T1 sagittal (four patients) or T1 coronal (three patients) images. In three patients, T2 coronal images were also obtained. T1-weighted images were obtained with inversion-recovery (IR) sequences of 1500/450/20–45 (TR/IR/range of TEs) or spin-echo (SE) sequences of 400–600/20–35/4 (TR range/

TE range/excitations). T2-weighted images were obtained with dual SE sequences of 2000/60,120/2 (TR/first-echo TE, second-echo TE/ excitations). All IR and SE images were obtained with the multislice technique and slice thicknesses of 5 or 7 mm.

Partial-saturation gradient-recalled echo (GRE) sequences were used in three patients with techniques previously described [11]. In summary, the MR signal is read out as a GRE rather than as an SE. T1-weighted GRE images, 100/15, were obtained with a large RF pulse angle (120°). T2-weighted GRE images, 100–120/30, 50, 100, were obtained with a small RF pulse angle (20°). These images were obtained by using a single-slice technique in the axial plane. Both a single T1 GRE and a series of three T2 GRE images were obtained in each patient studied with this technique.

Proton chemical-shift information was obtained in two patients with a modification of the method used by Dixon [12], previously described by Buxton et al. [13]. By using a TR of 500 msec and a TE of 50 msec, a series of images was obtained with progressive offsets of the 180° RF pulse. Given the known differences in the angular frequency of fat and water protons, through the variation of offsets, images can be acquired with total signal representing either the summation or the subtraction of these two populations of protons. A progressive increase in offset from 0 to 10.64 msec at increments of 2.66 msec generates a series of five images in which the fatty and water protons are alternatively in and out of phase. From these images obtained in the axial plane, the signal intensity of a region of interest (ROI) was determined and these data were analyzed (Fig. 1).

CT examinations were performed on third- and fourth-generation scanners. Contiguous 2- to 5-mm axial sections were obtained through the petrous bones in all cases. In addition, contiguous 4- to 5-mm direct coronal sections were obtained through the petrous bones in two patients. Examinations after IV administration of contrast material (43 g iodine) were performed in all patients. Nonenhanced examinations were also available in three patients.

Fig. 1.—Case 1: Chemical-shift imaging of recurrent cholesterol granuloma in right petrous region.

A, In-phase image, SE 500/50, 0-msec offset, represents summation of signal from fat and water protons.

B, Out-of-phase image, SE 500/50, 2.66-msec offset, represents difference of signal from fat and water protons and shows a reduction of signal in structures containing both fat and water protons, such as bone marrow, and a cancellation of signal at fat/water interfaces; for example, lateral rectus muscle and intraorbital fat (arrow). Although signal intensity of cholesterol granuloma does not appear to differ between the two images, a region-of-interest measurement in the center of the lesion showed the signal intensity in B was lower than in A.

A   B
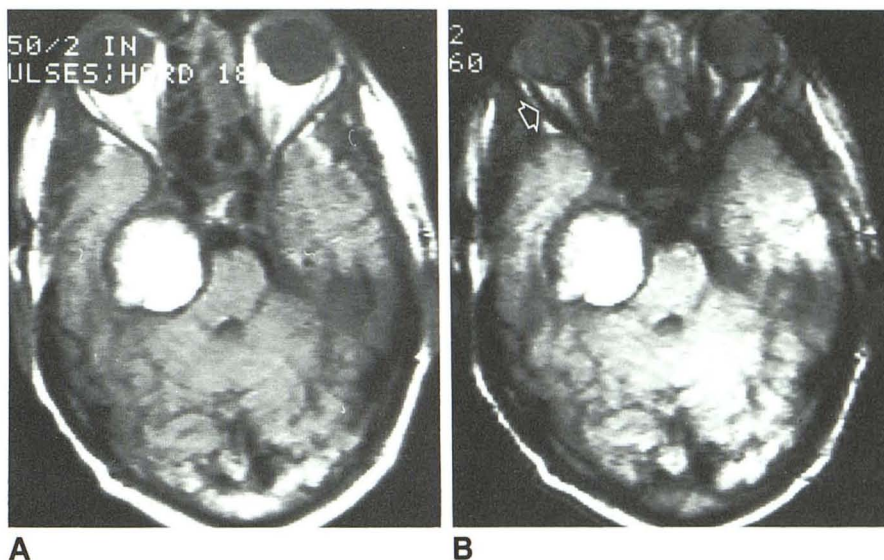
Results

MR examinations of five preoperative patients (a total of seven granulomas) and of one patient with symptomatic recurrence of a single lesion showed the lesions to have central regions of increased signal intensity on both T1- and T2-weighted images. The central portion of the abnormalities appeared homogeneous in three of eight instances on both T1- and T2-weighted images. In two cases, the central portions were homogeneous on T1-weighted images but slightly heterogeneous on T2-weighted images, with small focal areas of decreased signal intensity (Fig. 2). In the other three lesions, either linear septations or definite punctate regions of decreased signal intensity were identified on both T1- and T2-weighted images (Fig. 3). The peripheral aspect of the lesion demonstrated markedly decreased signal intensity in all instances on T2-weighted sequences and in three of eight lesions on T1-weighted images.

Partial-saturation GRE images were obtained in three of these patients. On all GRE sequences, the central portion of the lesion was of increased signal intensity. The peripheral aspect of the lesion demonstrated decreased signal intensity, and, as the TE was increased, the width of this ring progressively increased (Fig. 4). Proton chemical-shift imaging was used in two of these patients. In both instances, the signal intensity of an ROI within the central region of the lesion demonstrated a cyclic pattern of signal intensity (Fig. 5). These results indicate the presence of a population of fatty protons within the lesion.

In two recently treated patients and one asymptomatic patient treated 8 years earlier, the signal intensity of the central portion of the lesions was markedly reduced on T1-weighted images (Figs. 5 and 6). In two cases there remained increased signal on the T2-weighted images and in one case there was decreased signal on the T2-weighted images. Chemical-shift data, with an ROI defined within the central portion of the lesion, demonstrated no cyclic variation as the

offset of the 180° refocusing pulse progressed, indicating no central lipid component to the abnormality (Fig. 5).

CT examinations revealed the presence of well-defined, sharply marginated bony expansile lesions arising from the region of the petrous apex (Figs. 2, 3, and 6). A thin, often discontinuous, peripheral calcified rim was identified in eight of nine lesions. Fine peripheral enhancement, thought to be dural, was recognizable in two of three patients for whom both plain and enhanced scans were available. The central portion of the lesion was approximately the same density as adjacent brain in all patients except one in whom the mass was of slightly lower density. Three lesions were more complex and demonstrated a multilobulated configuration with fine, discontinuous calcified septa separating the components (Fig. 3). Displacement of the internal carotid artery was resolvable in seven of nine lesions.

Discussion

Cholesterol granulomas consist of a mass of inflammatory tissue that develops in response to the presence of cholesterol crystals [1–4]. The lesions are encountered most often in the middle ear or the mastoid air cells after obstruction of these normally aerated spaces due to associated diseases such as acute and chronic otitis media, granulomatous mastoiditis, and cholesteatoma [2, 3, 14]. The cholesterol granulomas that arise in the middle ear and mastoid tend to be small because they are detected early from the symptoms caused by the associated ear diseases [8, 10]. Cholesterol granulomas of the petrous apex, on the other hand, are not necessarily associated with other diseases and apparently grow silently over a period of years. Once these lesions reach a critical size, they may present as a cerebellopontine angle syndrome, causing compression and displacement of cranial nerves. It is estimated that one symptomatic cholesterol granuloma of the petrous apex occurs for every 30 acoustic
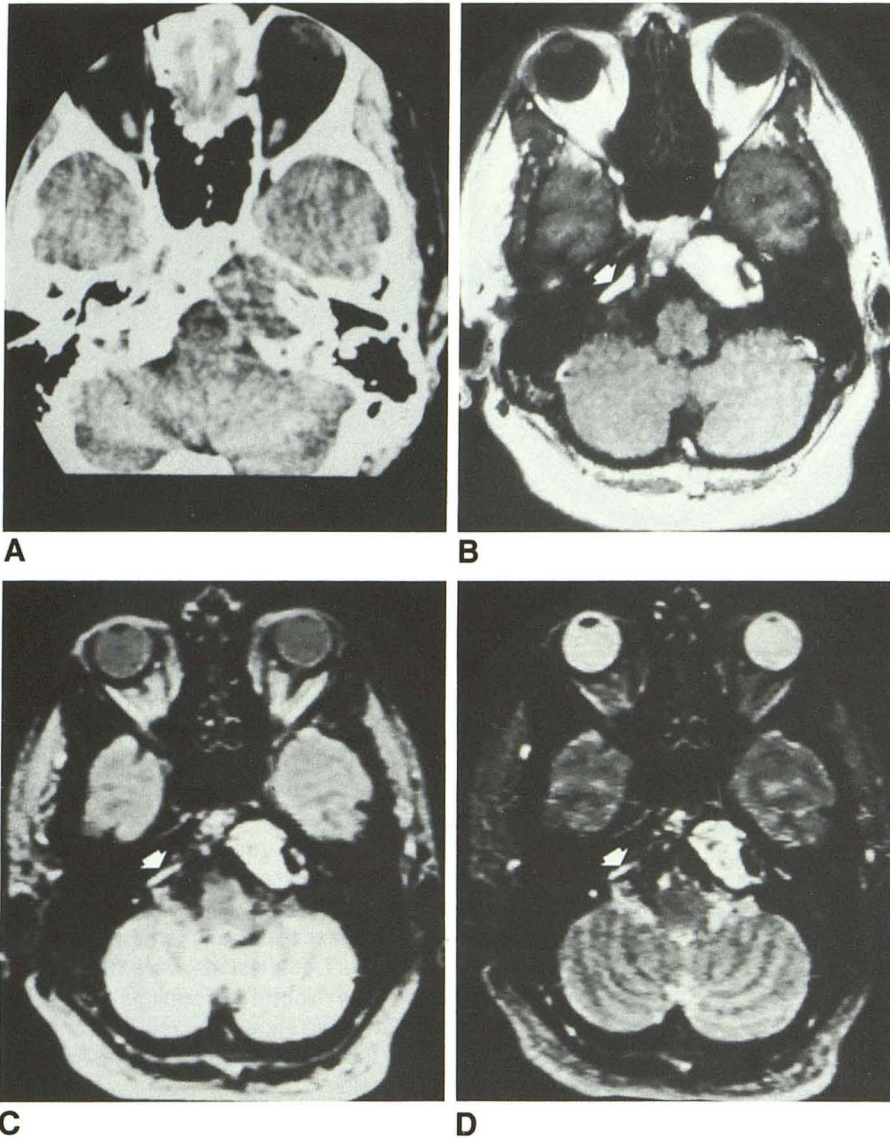
Fig. 2.—Case 5: Cholesterol granuloma of left petrous apex.

A, Nonenhanced CT scan shows well-defined, expansile, lytic lesion.

B–D, T1-weighted, 500/20 (B), and T2-weighted, 2000/60 (C) and 2000/120 (D), MR images. Lesion has central high signal intensity. Small cholesterol granuloma in right petrous apex (arrows) was asymptomatic.
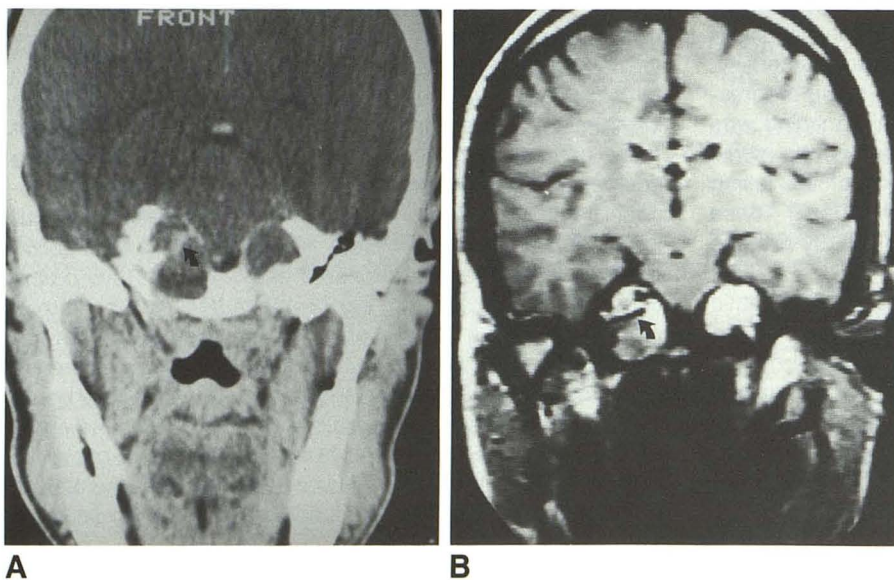

Fig. 3.—Case 6: Bilateral cholesterol granulomas of petrous bones.

A, Contrast-enhanced CT scan. Right-sided granuloma appears multilobulated, showing hyperdense septation (arrow).

B, T1-weighted MR image, SE 500/32, shows corresponding region of low signal intensity (arrow). Left-sided lesion appears more homogeneous without any definite septations.

Fig. 4.—Case 1: Recurrent cholesterol granuloma of right petrous apex. Partial-saturation gradient-recalled echo (GRE) series.

A, T1-weighted GRE image, 100/15 (120° flip angle).

B–D, T2-weighted GRE images, 100/30 (B), 100/50 (C), and 120/100 (D) (20° flip angles).

Peripheral ring of low signal intensity encircles lesion. This ring progressively enlarges with lengthening of TE secondary to local increase in magnetic susceptibility. Findings suggest hemosiderin-laden macrophages in peripheral fibrous wall of lesion. Alternatively, they may reflect iron within thin rim of mineralization noted around lesion on CT.

A   B

C   D
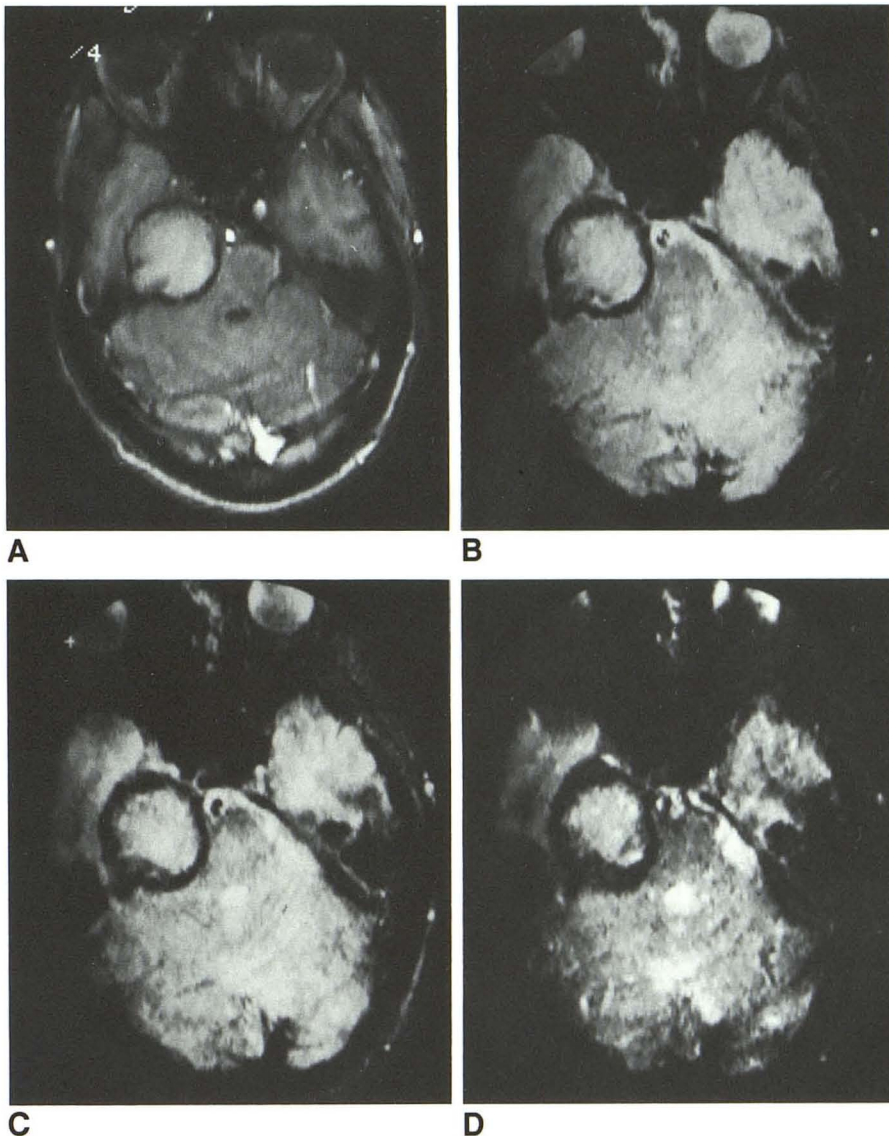
neuromas [8], making it the most common benign lesion of the petrous apex.

These lesions have characteristic gross and microscopic appearances. Grossly, these lesions simulate grains of popcorn with yellow and white areas. They usually contain golden or brownish fluid or semisolid material with glistening yellow cholesterol crystals. Histologically, they consist of fibrous tissue containing cholesterol clefts, an extensive inflammatory infiltrate, and evidence of chronic hemorrhagic products, including hemosiderin-laden macrophages. This entity is distinct from the primary cholesteatoma (epidermoid cyst), with which it is often confused. Primary cholesteatoma contains pearly white, friable keratotic material and a squamous epithelial wall, and there may or may not be an associated small cholesterol granuloma [8, 15].

The cause of cholesterol granulomas of the petrous apex is unknown, but a disease mechanism based on obstruction of air cells has been proposed [2, 14]. According to this theory, chronic obstruction to ventilation and drainage of pneumatized spaces in the petrous tip results in the development of negative pressure within the chamber. This process causes mucosal edema and rupture of blood vessels. In the absence of normal drainage, cholesterol derived from RBC membranes and other blood lipids reaches a sufficient concentration to result in crystalline forms. The cholesterol crystals incite a chronic inflammatory and foreign-body response, which may result in further blood vessel damage and recurrent hemorrhages. A vicious circle develops that results in a slowly growing lesion that may produce pressure erosion of bone.

Experimental models support the outlined pathogenesis of cholesterol granuloma. Ojala [16] and Beaumont [17] induced the development of cholesterol granulomas by producing negative pressure in the normally pneumatized chick humerus by obstructing ventilation. Main et al. [4] also induced the formation of this lesion in the mastoid cavity of squirrel
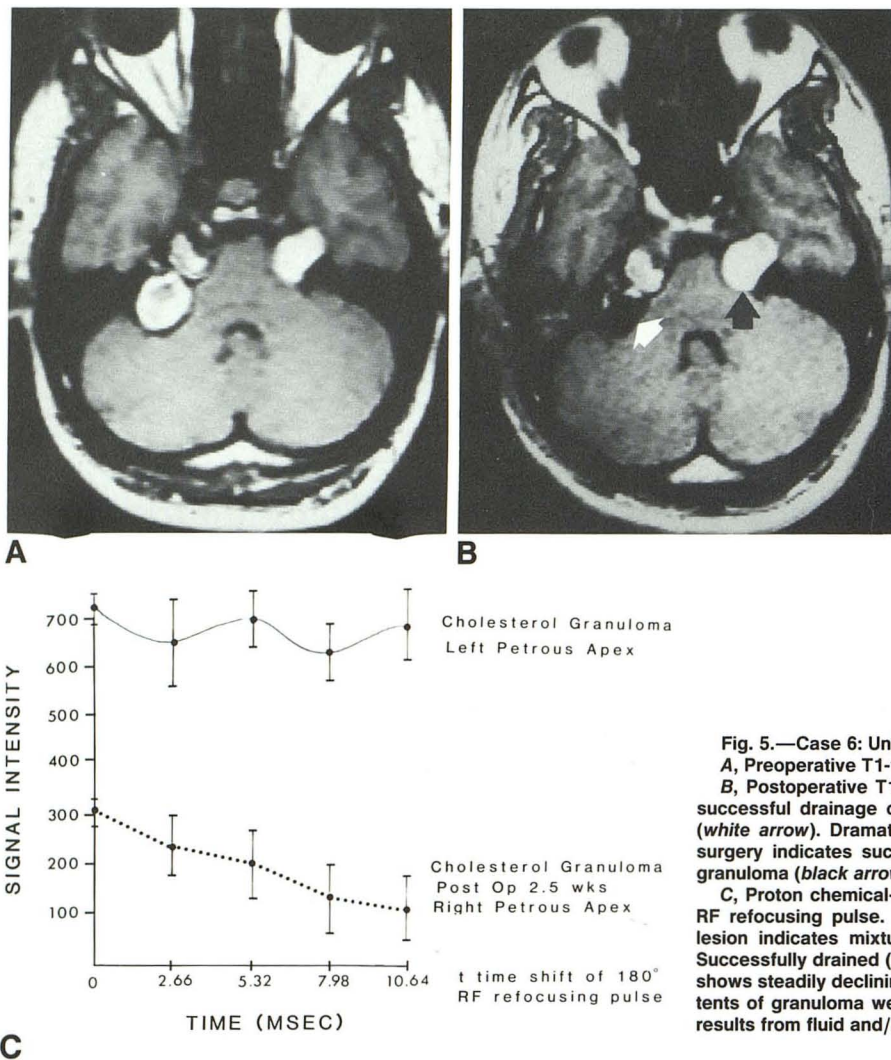
A   B

C

Fig. 5.—Case 6: Untreated and treated cholesterol granulomas.
A, Preoperative T1-weighted MR image, SE 500/32.
B, Postoperative T1-weighted MR image, SE 500/20, 2½ weeks after successful drainage of posterior portion of right cholesterol granuloma (white arrow). Dramatic decrease in signal intensity of granuloma after surgery indicates successful drainage. Untreated left-sided cholesterol granuloma (black arrow).
C, Proton chemical-shift data: signal intensity vs time (t) shift of 180° RF refocusing pulse. Cycling of signal intensity in untreated left-sided lesion indicates mixture of water and aliphatic portions within lesion. Successfully drained (Post Op) component of right lesion after 2½ weeks shows steadily declining curve without cycling. Presumably, aliphatic contents of granuloma were evacuated during drainage, and residual signal results from fluid and/or air that accumulated at surgical site.

monkeys by chronically obstructing the eustachian tubes. In addition, Friedmann [1] incited development of cholesterol granulomas by injecting sterile suspensions of cholesterol into the middle ear cavity of guinea pigs.

Radiologic observations also support this pathogenesis. Prominent pneumatization of the petrous apex has been recognized as a predisposing factor in the development of this lesion [8–10]. Pneumatization of the petrous bone usually is symmetric [18]; therefore, it is not surprising that two of our patients had bilateral lesions and three patients with unilateral lesions demonstrated extensive pneumatization of the contralateral uninvolved apex. These findings have been observed in other series [8, 9].

An accurate preoperative diagnosis of cholesterol granuloma is critical for appropriate surgical planning [5–10]. At our institution, surgical treatment of these lesions involves drainage and permanent fistulization of the lesion to the sphenoid or mastoid sinus via the transethmoid, transphenoid route or the transcochlear or retrocochlear route. These procedures are simple and require short hospitalizations. In contrast,

other lesions in this location require difficult and complicated surgery for excision or diagnostic biopsy [7, 8, 10]. For this reason, a specific and reliable preoperative diagnosis is extremely helpful to the surgeon.

CT scanning has been the major method used to help establish the preoperative diagnosis of cholesterol granuloma [6–10]. As demonstrated in our series of seven patients and in other series [8–10], this lesion typically presents as a sharply marginated, expansile lesion in the petrous apex. Both erosion involving the petrous apex, the lateral aspect of the clivus, the jugular tubercle, the anterior carotid canal, and the internal auditory canal was noted in the majority of patients. These CT findings are characteristic of a cholesterol granuloma; however, they are not specific. Other benign and malignant lesions can mimic these findings on CT [8–10, 15]. The differential diagnosis of expansile lesions in this location includes primary cholesteatomas (epidermoids), mucoceles, histiocytosis X, neuromas, carotid aneurysms, and primary bone and cartilage neoplasms [7–10]. In Figure 7 a contrast-enhanced CT scan of a grade 1 chondrosarcoma demon-

Fig. 6.—Case 4: Pre- and postoperative appearance of cholesterol granuloma.

A, Preoperative nonenhanced CT scan.

B, Preoperative T1-weighted SE image, 600/35.

C, Postoperative nonenhanced CT scan 2 months after successful drainage and permanent fistulization of cholesterol granuloma. There is no dramatic change in size of lesion.

D, Postoperative T1-weighted IR image, 1500/450/45. A striking decrease is seen in signal intensity of cholesterol granuloma, indicating drainage of cholesterol crystals and hemorrhagic products from lesion.

A

B

C

D
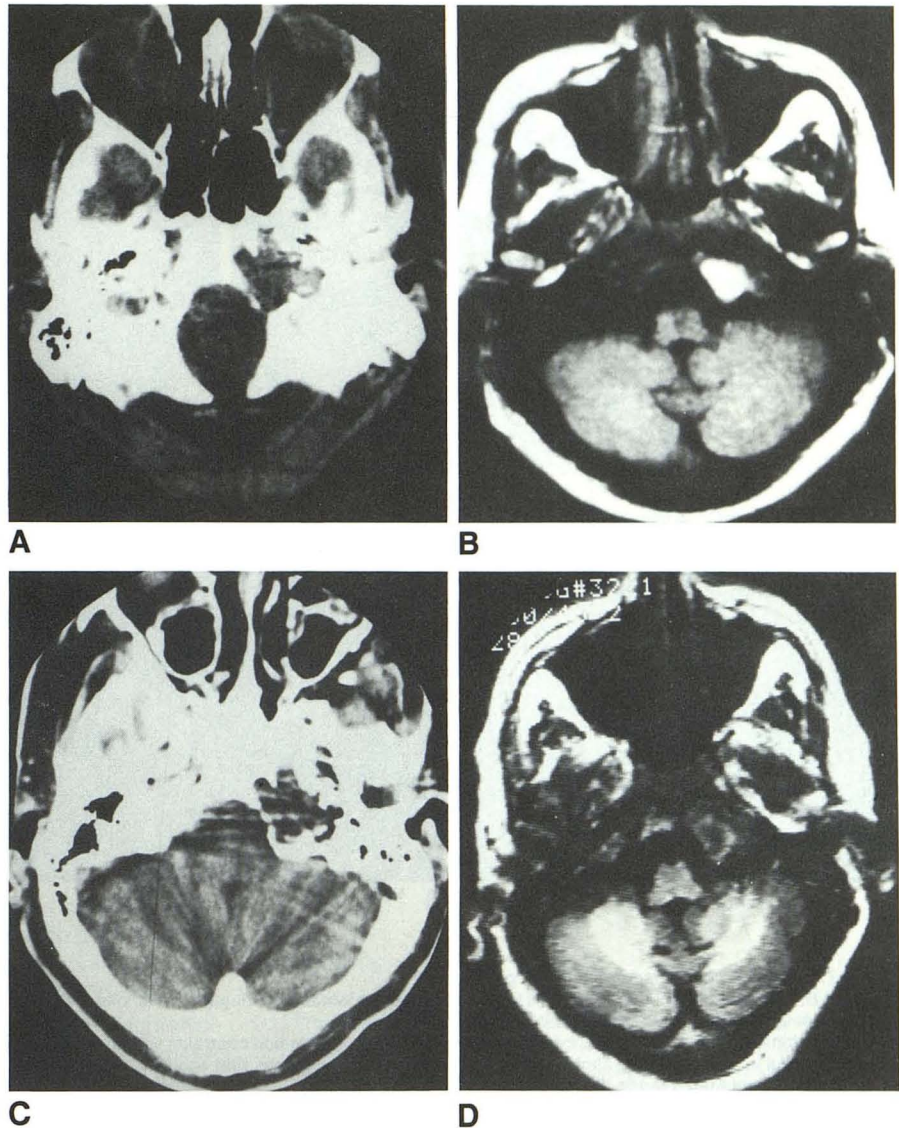
strates an appearance similar to that in most of our cases of cholesterol granuloma.

Cholesterol granuloma of the petrous apex has a very characteristic appearance on conventional MR studies (Figs. 2, 3, 5, and 6). This lesion consistently demonstrated central regions of short T1 and prolonged T2 in all five patients who underwent preoperative MR examinations. In addition, one patient who developed a symptomatic recurrence of a single lesion also demonstrated similar signal characteristics. The rather unique increased signal intensity on T1-weighted images of these lesions presumably is due to the unusual combination of cholesterol crystals, chronic hemorrhagic products, and proteinaceous debris seen in the cholesterol granuloma. It is unclear which component is primarily responsible for the increased signal intensity on the T1-weighted image; however, one group [19] postulates that the chronic hemorrhagic products are the primary source. Our data cor-

roborate the MR findings of other reports [9, 10, 19] of cholesterol granulomas of the petrous apex that showed increased signal intensity on both T1- and T2-weighted images.

Occasionally, it can be difficult to distinguish a small cholesterol granuloma from normal marrow in the clivus or petrous apex because both demonstrate increased signal intensity on T1-weighted images. However, these two entities can be readily differentiated by examining the proton density and T2-weighted images. Whereas marrow fat demonstrates a progressive decrease in signal intensity with increased T2-weighting, a cholesterol granuloma maintains a high signal intensity on T2-weighted images (Fig. 2).

MR appears to be more specific than CT in establishing the correct preoperative diagnosis of cholesterol granuloma. Although cholesterol granulomas demonstrate central components with short T1 and prolonged T2, the vast majority of
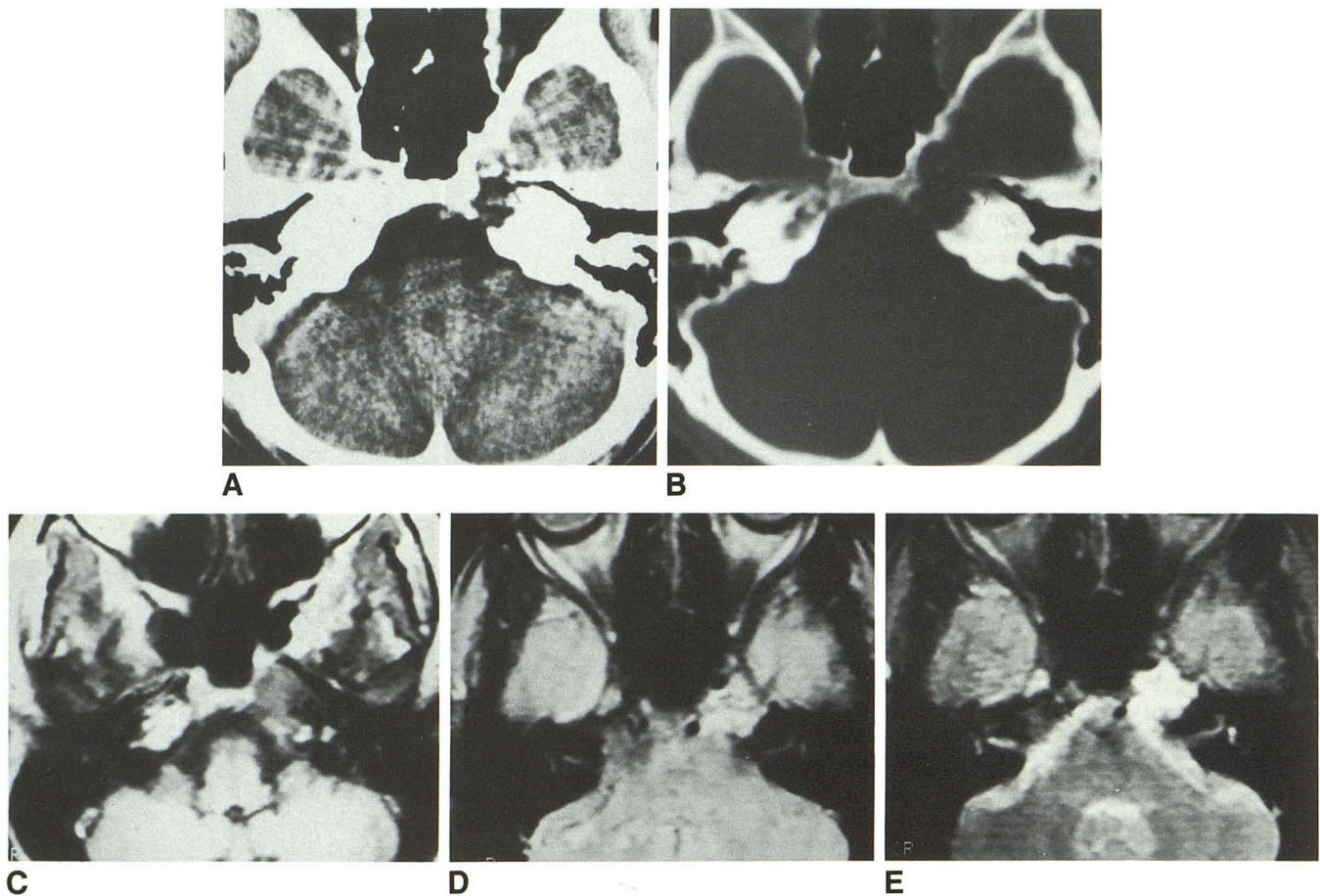
Fig. 7.—Grade 1 chondrosarcoma of left petrous apex.
   A and *B*, Contrast-enhanced CT scan (*A*) and CT with bone window setting (*B*). Lytic expansile lesion in left petrous apex is virtually indistinguishable from typical CT appearance of cholesterol granuloma.
   C, T1-weighted SE image, 400/20. Intermediate signal intensity of lesion contrasts with increased signal intensity of cholesterol granuloma. T1-weighted image is useful in differentiating cholesterol granuloma from other lesions that occur at this site.
   D and *E*, T2-weighted images, SE 2000/60 (*D*) and SE 2000/120 (*E*). Grade 1 chondrosarcoma resembles cholesterol granuloma. T2-weighted images do not aid in differential diagnosis.

other lesions in the differential diagnosis of expansile masses in the petrous apex demonstrate prolonged T1 and T2 [15, 19] (i.e., most primary cholesteatomas, metastases, neuromas, and primary bone and cartilage tumors [Fig. 7], and histiocytosis X). In the case of an arterial aneurysm, MR would be expected to show the combination of flow voids with subacute and chronic thrombosis [19]. Thus, cholesterol granulomas can be distinguished from most lesions in this location by its characteristic signal intensity on conventional MR studies.

Although the MR appearance of cholesterol granuloma is quite characteristic, it is not pathognomonic. Gentry et al. [19] described one atypical acoustic neuroma and one thrombosed aneurysm that demonstrated increased signal intensity on T1- and T2-weighted images in their series of 75 cerebellopontine angle and petromastoid lesions. Also, two acquired

cholesteatomas of the tympanomastoid region [19] and one primary cholesteatoma of the epitympanum [15] have been described as having a short T1 and long T2. Although all primary cholesteatomas of the petrous apex described to date have demonstrated a prolongation of both T1 and T2 [15], it is probable that a primary cholesteatoma in the petrous apex eventually will be described that has a short T1, as has occurred in primary and secondary cholesteatomas of the tympanic region. Similarly, a mucocele in the petrous apex would be expected to demonstrate a signal intensity similar to that of cholesterol granuloma [10], although no example of this has been described to date in this location.

An atypical acoustic neuroma should be distinguished from a cholesterol granuloma by a contrast-enhanced CT examination, but the other lesions—thrombosed aneurysm, primary cholesteatoma, and mucocele—would, in theory, be difficult

to differentiate from a cholesterol granuloma with CT and conventional MR examinations. Specialized MR pulse sequences, including partial-saturation GRE imaging in three patients and proton chemical-shift imaging in two patients with cholesterol granulomas, were utilized in an attempt to improve the diagnostic specificity of MR by further characterizing these lesions. GRE imaging in all three patients demonstrated an enlarging peripheral ring of decreased signal intensity as the TE was lengthened from 15 to 100 msec (Fig. 4). This technique is extremely sensitive to the effects of magnetic field inhomogeneities [11]. This finding indicates evidence of a peripheral, but not central, magnetic susceptibility effect, suggesting the presence of hemosiderin-laden macrophages in the fibrous wall of the lesion. A thrombosed aneurysm could conceivably demonstrate this peripheral magnetic susceptibility effect, but acoustic neuromas, primary cholesteatomas, and mucoceles would not be expected to demonstrate peripheral susceptibility. Proton chemical-shift imaging was also performed in two patients, one with a preoperative lesion (Fig. 5) and one with a clinically recurrent lesion (Fig. 1). In both instances, the central region of the lesion demonstrated a cyclic pattern of signal intensity as the aliphatic and water protons were sequentially measured in- and 180° out-of-phase. This cyclic pattern of signal intensity indicates the presence, in vivo, of a mixed population of aliphatic (CH_2) and H_2O protons within the lesions [12, 13]. The aliphatic protons presumably reflect the lipids and cholesterol crystals within these lesions. Although a primary cholesteatoma could also conceivably demonstrate a cyclic pattern of signal intensity in proton chemical-shift imaging, since these lesions also contain cholesterol centrally, an acoustic neuroma, mucocele, and thrombosed aneurysm would not be expected to demonstrate this effect, as these lesions usually do not contain visible aliphatic protons [3]. Thus, the combination of GRE imaging and proton chemical-shift imaging enhances the diagnostic specificity of MR of cholesterol granulomas by distinguishing this lesion from other lesions that can have a similar appearance on both CT and conventional MR examinations.

Postoperative MR examinations were performed in three clinically successfully drained and marsupialized lesions. Two patients were examined 2½ weeks and 2 months, respectively, after successful drainage and fistulization to the mastoid sinus, while one patient was examined 8 years after successful surgical drainage and permanent fistulization to the sphenoid sinus. In all three treated lesions, there was a marked decrease in signal intensity on T1-weighted images compared with the preoperative appearance available in two of the cases (Figs. 5 and 6). In addition, the proton chemical-shift imaging series demonstrated the absence of cycling of signal intensity in two of the patients, indicating no central lipid component in the abnormality (Fig. 5). The lengthening of the T1 of the abnormality and the absence of aliphatic protons centrally on chemical-shift examination undoubtedly reflect the successful evacuation of the cholesterol crystals and chronic hemorrhagic products from the granuloma. Although MR can demonstrate a significant alteration in signal intensity in successfully treated lesions within a period of 2½

weeks (Fig. 5), we observed one patient (case 2) in whom CT did not demonstrate substantial morphologic change for a period of 1 year, with slow involution subsequently noted. These observations suggest that MR is more sensitive than CT in demonstrating successful treatment of these lesions and that MR probably is the method of choice for follow-up evaluation of these lesions after surgical treatment for early detection of recurrent lesions.

In conclusion, MR appears to be more specific than CT in establishing the diagnosis of cholesterol granuloma before surgery. A mass in the petrous apex that demonstrates short T1, prolonged T2, peripheral magnetic susceptibility, and evidence of aliphatic protons centrally will virtually always be a cholesterol granuloma, as no other mass in this location would be expected to demonstrate all of these MR characteristics. In the vast majority of cases, the diagnosis of a cholesterol granuloma can be established by using conventional T1- and T2-weighted studies alone. On rare occasions in which a cholesterol granuloma needs to be differentiated from a thrombosed aneurysm, hemorrhagic mass, mucocele, or atypical neuroma located in the petrous apex region, chemical-shift and GRE studies would be useful adjuvant studies. MR also appears to be the technique of choice for the follow-up evaluation of cholesterol granuloma after surgical treatment. The dramatic decrease in signal intensity within the lesion on T1-weighted images after surgical intervention can be useful in confirming that a lesion has been successfully evacuated. Conversely, the development of increased signal intensity on T1-weighted images in a treated patient would suggest the development of a recurrent lesion.

REFERENCES

1. Friedmann I. Epidermoid cholesteatoma and cholesterol granuloma: experimental and human. *Ann Otol Rhinol Laryngol* **1959**;68:57–79
2. Nager GT, Vanderveen TS. Cholesterol granuloma involving the temporal bone. *Ann Otol Rhinol Laryngol* **1976**;85:204–209
3. Barnes L, Peel RL. Diseases of external auditory canal, middle ear, and temporal bone. In: Barnes L, ed. *Surgical pathology of the head and neck*, vol. 1. New York: Marcel Dekker, **1985**:470–473, 662–663
4. Main TS, Shimada T, Lim DJ. Experimental cholesterol granuloma. *Arch Otolaryngol Head Neck Surg* **1970**;91:356–359
5. Gacek RR. Diagnosis and management of primary tumors of the petrous apex. *Ann Otol Rhinol Laryngol* [*Suppl*] **1975**;18:1–20
6. Montgomery WW. Cystic lesions of the petrous apex: transsphenoidal approach. *Trans Am Otol Soc* **1977**;65:32–39
7. Gacek RR. Evaluation and management of primary petrous apex cholesteatoma. *Otolaryngol Head Neck Surg* **1980**;88:519–523
8. Lo WWM, Solti-Bohman LG, Brachman DE, Gruskin P. Cholesterol granuloma of the petrous apex: CT diagnosis. *Radiology* **1984**;153:705–711
9. Latack JT, Graham MD, Kemink JL, Knake JE. Giant cholesterol cysts of the petrous apex: radiologic features. *AJNR* **1985**;6:409–413
10. Amedee RG, Marks HW, Lyons GD. Cholesterol granuloma of the petrous apex. *Am J Otol* **1987**;8(1):48–55
11. Edelman RR, Johnson K, Buxton R, et al. MR of hemorrhage: a new approach. *AJNR* **1986**;7:751–756
12. Dixon WT. Simple proton spectroscopic imaging. *Radiology* **1984**;153:189–194
13. Buxton RB, Wismer GL, Brady TJ, Rosen BR. Quantitative proton chemical shift imaging. *Magn Reson Med* **1986**;3:881–900
14. House JL, Brackmann DE. Cholesterol granuloma of the cerebellopontine

      angle. *Arch Otolaryngol Head Neck Surg* **1982**;108:504–506

15. Latack JT, Kartush JM, Kemink JL, Graham MD, Knake JE. Epidermoido-
    mas of the cerebellopontine angle and the temporal bone: CT and MR
    aspects. *Radiology* **1985**;157:361–366

16. Ojala L. Pneumatization of the bone and environmental factors: experi-
    mental studies on chick humerus. *Acta Otolaryngol* [*Suppl*] (Stockh)
    1957;133

17. Beaumont GD. The effect of exclusion of air from pneumatized bones. *J
    Laryngol Otol* **1966**;80:236

18. Allam AF. Pneumatization of the temporal bone. *Ann Otol Rhinol Laryngol*
    1969;78:49–64

19. Gentry LR, Jacoby CG, Turski PA, Houston LW, Strither CM, Sackett JF.
    Cerebellopontine angle—petromastoid mass lesions: comparative study
    of diagnosis with MR imaging and CT. *Radiology* **1987**;163:513–520